bioRxiv preprint doi: https://doi.org/10.1101/2021.08.04.454918; this version posted August 5, 2021. The copyright holder for this preprint (which was not certified by peer review) is the author/funder. All rights reserved. No reuse allowed without permission.

The role of Musashi-1 in CEP290 c.2991+1655A>G cryptic exon splicing in Leber Congenital Amaurosis

Daniele Ottaviani[1,2,3], Amelia Lane[1], Katarina Jovanovic[1], Jessica C. Gardner[1], Paul E. Sladen[1], Kwan L. Hau[1], Anna Brugulat Panes[1], Rosellina Guarascio[1], Alison J. Hardcastle[1], Michael E. Cheetham[1,*].

[1]UCL Institute of Ophthalmology, 11-43 Bath Street, London EC1V 9EL, UK

[2]Department of Biology, University of Padua, Via Ugo Bassi 58/B, 35121 Padua, Italy

[3]Veneto Institute of Molecular Medicine, Via Giuseppe Orus 2, 35129 Padua, Italy

*Correspondence: michael.cheetham@ucl.ac.uk

HIGHLIGHTS

- The human retina expresses a unique set of gene isoforms
- Musashi-1 regulates alternative splicing in 3D human retinal organoids
- Musashi-1 knockdown in 3D retinal organoids affects gene splicing and homeostasis in photoreceptors
- Musashi-1 may regulate alternative splicing of cryptic exons in retina but not in LCA10

KEYWORDS

Musashi-1, MSI1, alternative splicing, retina, CEP290, LCA10, RNA, antisense, isoform, deep intronic variant

bioRxiv preprint doi: https://doi.org/10.1101/2021.08.04.454918; this version posted August 5, 2021. The copyright holder for this preprint (which was not certified by peer review) is the author/funder. All rights reserved. No reuse allowed without permission.

SUMMARY

Human photoreceptors maximise alternative exon splicing to generate a unique set of gene isoforms. Conversely, the inclusion of a cryptic exon caused by the c.2991+1655A>G deep intronic change in *CEP290* occurs in the human retina leading to Leber Congenital Amaurosis (LCA10). The RNA-binding protein Musashi-1 (MSI1) is a key component of alternative splicing in the developing mouse retina. Here we investigated the role of MSI1 in human photoreceptor-specific splicing and its potential role in *CEP290* aberrant splicing disease. Alternative splicing was studied using human induced pluripotent stem cell derived 3D retinal organoid and RPE RNA-seq datasets and several photoreceptor gene isoforms were identified. Their temporal expression was resolved in control 3D retinal organoids in comparison to development and differentiation markers. Morpholino knockdown of *MSI1* in control retinal organoids reduced the expression of several photoreceptor differentiation markers and the inclusion of photoreceptor-specific exons. Nonetheless, *MSI1* knockdown in homozygous CEP290 c.2991+1655A>G LCA10 retinal organoids did not affect the inclusion of the LCA10-associated cryptic exon. These results show that while MSI1 is important for photoreceptor alternative splicing and homeostasis, it is not a major driver of the recognition of the CEP290 cryptic splice site and the manifestation of LCA10.

bioRxiv preprint doi: https://doi.org/10.1101/2021.08.04.454918; this version posted August 5, 2021. The copyright holder for this preprint (which was not certified by peer review) is the author/funder. All rights reserved. No reuse allowed without permission.

INTRODUCTION

The human retina is highly specialised, multi-layered sensory neural tissue with tightly regulated gene expression, especially during differentiation and development. The ability to model human inherited retinal disease through patient stem cell derived retinal organoids (RO) has created unprecedented opportunities to understand key processes occurring during retinal development and degeneration. ROs can be developed from human induced Pluripotent Stem Cells (hiPSC) obtained from patients and healthy controls thus allowing the modelling of rare and complex retinal diseases in a human context *in vitro* (Lancaster and Knoblich, 2014). In 2016, ROs were used to study the most common autosomal-recessive form of Leber Congenital Amaurosis (LCA), which is caused by the c.2991+1655A>G deep intronic change in the *CEP290* gene (CEP290-LCA or LCA10) (Parfitt et al., 2016). CEP290 is localised at both the centrosome and cilia and is regarded as an essential gatekeeper during transport of cargo across the transition zone of photoreceptor primary cilia (Craige et al., 2010). The c.2991+1655A>G change introduces a hypomorphic cryptic splice-site in *CEP290* that leads to the retention of a 128 bp pseudo-exon in the mature transcript to a premature stop codon p.Cys998* and a net loss of about 50% of the wildtype (WT) CEP290 mRNA in fibroblasts (den Hollander et al., 2006; Dulla et al., 2018; Ruan et al., 2017). Although the level of *CEP290* mRNA aberrant splicing is too low in most tissues to cause syndromic disease, the inclusion of the pseudo-exon in retina increases to over 80% of the total *CEP290* transcript in patient derived ROs, leading to a greater reduction in functional CEP290 protein potentially explaining the retinal susceptibility to LCA10 (Dulla et al., 2018; Parfitt et al., 2016). The increase in *CEP290* aberrant splicing correlated with the inclusion of retinal specific exons of *BBS8* and *RPGR*, suggesting this switch might be related to photoreceptor differentiation and

bioRxiv preprint doi: https://doi.org/10.1101/2021.08.04.454918; this version posted August 5, 2021. The copyright holder for this preprint (which was not certified by peer review) is the author/funder. All rights reserved. No reuse allowed without permission.

specialisation (Parfitt et al., 2016). Therefore, we wanted to understand the molecular machinery that regulates splicing in the retina, timing of splice switching to retinal isoforms, and aberrant splicing such as CEP290-LCA in LCA10.

In 2016, Murphy and colleagues found that novel transcript isoforms were expressed in mouse retina and characterised the transcriptome. They identified the RNA-binding protein (RBP) Musashi-1 (MSI1) as a driver of alternative splicing (AS) and retinal-specific exons were found to be enriched in MSI1 binding motifs downstream of the splicing donor site (Murphy et al., 2016). MSI1, an RBP which targets UAG motif-enriched regions, is named after the Japanese swordsman and rōnin Miyamoto Musashi who is often portrayed holding two swords in his belt in a V-shape layout. Similarly, Drosophila knockouts for *MSI1* develop two bristles in their compound eye "ommatidia" thus resembling Musashi's swords (Nakamura et al., 1994). This highlights a key role for *MSI1* in eye development, as also demonstrated later in mouse retina (Susaki et al., 2009). Recently, *Msi1* and its paralog *Musashi-2* were shown to be required for photoreceptor morphogenesis and survival in mice (Sundar et al., 2020). Moreover, a role for both MSI1 and MSI2 has been reported in stem cell renewal and in cancer onset, progression and metastasis (Kudinov et al., 2017; Okano et al., 2005; Wuebben et al., 2012).

Recently, Ling and colleagues performed an extensive analysis of many of the RNA-seq datasets available in literature on mouse tissues and on the human Genotype-Tissue Expression (GTEx) project with two additional datasets from the human retina (Ling et al., 2020). This revealed a high degree of AS in neuronal cells, particularly in the retina. The retina transcriptome has a distinctive splicing pattern and expresses at least 30 specific, previously unannotated, in-frame exons and micro-exons. Furthermore, MSI1 was confirmed as a driver of retinal splicing, together with PTPB1,

bioRxiv preprint doi: https://doi.org/10.1101/2021.08.04.454918; this version posted August 5, 2021. The copyright holder for this preprint (which was not certified by peer review) is the author/funder. All rights reserved. No reuse allowed without permission.

and *MSI1* was found to be expressed mainly in rod photoreceptors thus making this mechanism likely photoreceptor specific.

Overall, these studies support the view that human photoreceptors maximise alternative exon splicing, leading to a highly specialised transcriptome during development and differentiation. This raises the possibility, however, that the retina could be particularly vulnerable to intronic mutations, compared to other tissues, as observed for the CEP290-LCA variant (Parfitt et al., 2016) and for variants within the introns of *ABCA4* that lead to Stargardt Disease (Khan et al., 2020). The mRNA processing mechanisms causing this retinal sensitivity to deep intronic variants resulting in aberrant splicing are still unknown.

In this study, we exploited RNA-seq from ROs and Retinal Pigment Epithelium (RPE) to identify the RO specific transcriptome. We aimed to correlate the inclusion of photoreceptor-specific exons and the CEP290-LCA pseudoexon with that of other AS exons, and to investigate the role of MSI1. We developed ROs to define the timing of the AS program during human retinal development *in vitro*. We then exploited Morpholino-mediated *MSI1* gene silencing. We show MSI1 is indispensable for the execution of the photoreceptor-specific splicing program in human retinal tissue but has a limited impact on the inclusion of the CEP290-LCA cryptic exon.

bioRxiv preprint doi: https://doi.org/10.1101/2021.08.04.454918; this version posted August 5, 2021. The copyright holder for this preprint (which was not certified by peer review) is the author/funder. All rights reserved. No reuse allowed without permission.

RESULTS

Identification of alternative splicing events unique to retinal organoids.

We recently developed an RNA-seq transcriptome for 3D ROs from a healthy donor (Lane et al., 2020); RPE from the same hiPSC line were differentiated in parallel and also sequenced by RNA-seq. The rMATS pipeline compares two experimental conditions and identifies patterns of exon skipping, alternative 5' and 3' splice site usage, mutually exclusive exons and retained introns (Shen et al., 2014). It was used to explore and compare the RO and RPE datasets to identify differentially expressed exons (AS events) and the potential photoreceptor transcriptome. We found 11,606 exons were differently spliced in ROs and many that were not previously annotated are reported here (Supplementary Table 1). Among the identified exons, 5074 were significantly upregulated in ROs while, 6532 were downregulated (Supplementary Table 1). Despite being enriched in photoreceptors, ROs contain many cell types of the human retina; namely Muller-Glia, retinal ganglion cells, interneurons (bipolar, horizontal, amacrine) and RPE (Collin et al., 2019). Furthermore, exons could be shared with other tissues as well. Therefore, we compared the AS exons with those from mice (Murphy et al., 2016) in order to narrow down the analysis to the common photoreceptor AS events and to test for exon conservation. The exon coordinates shortlisted by Murphy *et al.* were aligned by synteny to the human genome thus allowing filtering of our dataset for AS events that matched. We found 102 exons enriched in the human retina have mouse orthologues (Supplementary Table 2). From the top 20 most significant upregulated and downregulated orthologues displaying the highest inclusion difference between RO and RPE (Figure 1A, B), we initially focused on a previously unannotated micro-exon of 17bp in length in the *IMPDH1* gene (*IMPDH1* exon-14), shown in Figure 1A. In 2016, IMPDH1 exon-14 expression in the

bioRxiv preprint doi: https://doi.org/10.1101/2021.08.04.454918; this version posted August 5, 2021. The copyright holder for this preprint (which was not certified by peer review) is the author/funder. All rights reserved. No reuse allowed without permission.

human retina was reported by VastDB, an extensive database of alternative spicing events in vertebrates (Tapial et al., 2017). Among the 20 shortlisted exons, *IMPDH1* exon-14 was validated by Murphy and colleagues by RT-PCR in mouse retina, together with *CC2D2A* (Murphy et al., 2016). Although awaiting validation in humans, *IMPDH1* exon-14 showed the strongest MSI1-dependent expression in mice (Murphy et al., 2016). Therefore, we selected the *IMPDH1*-exon 14 as a reporter to test when the AS switch occurs in RO development and to investigate if MSI1 is part of this mechanism of exon selection in the human retina.

Retinal-specific isoforms appear during retinal organoid development.

The expression of known markers of retinal differentiation was investigated in control ROs at different time-points of differentiation *in vitro*; day (D) 20, 40, 50, 60, 70, 90, 100, 120, 150 and 180 (Figure 2). RT-PCR showed that specifiers of retinal progenitor cells, *PAX6* and *VSX2/Chx10,* are concordantly and constantly expressed during RO differentiation and development from about D20 onwards (Figure 2A). In contrast, the photoreceptor-specific transcription factors *CRX*, *NRL* and *NR2E3* were detected at later timepoints showing an increase from D50, D70 and D90 onwards, respectively (Figure 2A). We next performed quantitative real-time PCR (qPCR) over the time-course of RO differentiation and extended our analysis to day 200. There was exponential increase in expression for the photoreceptor associated genes when the data were plotted on a semi-Log transformed scale (Figure 2B). The results showed a similar trend of exponential increase for the expression of *CRX*, *NRL* and *NR2E3* starting from D20 in ROs (Figure 2B), except for *PAX6* and *VSX2*, which were relatively constant.

bioRxiv preprint doi: https://doi.org/10.1101/2021.08.04.454918; this version posted August 5, 2021. The copyright holder for this preprint (which was not certified by peer review) is the author/funder. All rights reserved. No reuse allowed without permission.

These stages of RO development were used to characterize when retinal-specific exons are alternatively spliced in human retina. Retinal-specific isoforms have been previously described for *BBS8/TTC8*, *REEP6* and *RPGR* and mutations in these retinal exons have been linked to retinal degeneration (Arno et al., 2016; Kirschner et al., 1999; Murphy et al., 2015). Therefore, the expression of retinal-specific isoforms *BBS8* exon-2A, *REEP6.1*, *RPGRorf15* were investigated with the addition of *IMPDH1* exon-14 (Figure 3). There was consistent increase of *RPGRorf15* transcripts from D40, which preceded that of *REEP6.1* and *BBS8* exon-2A, which were first detected at D50 (Figure 3A). Transcripts containing Exon 14 of *IMPDH1* were detectable at D20 at the first stages of RO differentiation, suggesting the retinal splicing program might be active early during retinal development *in vitro* (Figure 3A). We performed a more resolved qPCR analysis and found *BBS8* exon-2A, *REEP6.1*, *RPGRorf15* and *IMPDH1* exon-14 are all detectable at D20 (Figure 3B). Notably, there was a close fit with markers of photoreceptor differentiation, *CRX*, *NRL* and *NR2E3,* whose transcription rate rise exponentially from D20. These results suggest the retinal splicing program is initiated early during RO development *in vitro* and qPCR yields the appropriate resolution of the inclusion of retinal-specific isoforms that seem to closely follow photoreceptor differentiation and development in ROs.

MSI1 knockdown affects photoreceptor gene expression.

We used an antisense oligonucleotide (Morpholino, *MSI1*-MO) to knockdown the expression of *MSI1* in mature ROs to study the role of MSI1 in retinal homeostasis. Control ROs were treated twice with 10 μM of *MSI1*-MO or 10 μM of a control non-specific MO over a 5-day period at D195 of development. This window of treatment was selected as the photoreceptors have completed development and were likely to

bioRxiv preprint doi: https://doi.org/10.1101/2021.08.04.454918; this version posted August 5, 2021. The copyright holder for this preprint (which was not certified by peer review) is the author/funder. All rights reserved. No reuse allowed without permission.

yield a high qPCR signal-to-noise ratio after treatment. *MSI1* downregulation was analysed by quantifying the mRNA level by qPCR (Figure 4A) and by plotting fold-changes in gene expression. This confirmed a statistically significant 50% reduction in the level of *MSI1* transcript (Figure 4A). The global markers of neuronal cell fate *VSX2* (Figure 4B) and *PAX6* (Figure 4C) were not altered by *MSI1* knock-down. In contrast, genes related to the photoreceptor cell lineage were significantly decreased, with the rod photoreceptor-specific genes *NRL* (Figure 4D) and *NR2E3* (Figure 4E) showing a 60% reduction and more affected than the cone-rod marker *CRX*, which showed a 40% decrease (Figure 4F). This suggests reduction of *MSI1* could affect photoreceptor homeostasis and survival, with possibly a greater impact on rod function when compared to cones.

MSI1 is important for alternative splicing in human retinal organoids.

We investigated the effect of *MSI1*-MO treatment on retina-specific exons that have previously been reported as containing consensus sites for MSI1 (Ling et al., 2020), starting with *IMPDH1* exon-14. The inclusion of *IMPDH1* exon-14 was analysed and was found to be significantly reduced by approximately 50% (Figure 5A). Furthermore, the retinal-specific exon 30 in the *CC2D2A* gene was also reduced, but exon 24 of *CC2D2A*, another retinal-specific exon in the same transcript was not reduced (Figure 5B). *CASK* and *ADGRV1* retinal exons were significantly decreased by 60% and 90%, respectively, in the *MSI1* knockdown ROs (Figure 5C, D), whereas *DOC2B* was not affected by *MSI1* knockdown as shown previously in mice (Figure 5E) (Ling et al., 2020). Surprisingly, we observed that *REEP6.1* splicing was also affected by MSI1 reduction (Figure 5F), which has not been previously reported as containing consensus sites for MSI1 (Ling et al., 2020). However, not all of the exons with MSI1

bioRxiv preprint doi: https://doi.org/10.1101/2021.08.04.454918; this version posted August 5, 2021. The copyright holder for this preprint (which was not certified by peer review) is the author/funder. All rights reserved. No reuse allowed without permission.

consensus sites were affected by the *MSI1*-MO in this assay. While *IMPDH1* exon-14, *CC2D2A* exon-30, *ADGRV1* and *CASK* show a splicing pattern strongly dependent on *MSI1* expression, an alternative mechanism likely exists for other retinal exons such as *CC2D2A* exon-24 and *DOC2B*.

MSI1 drives photoreceptor-specific splicing in human retinal organoids.

Murphy and colleagues identified the MSI1-driven AS in mouse retina; whereas, Ling and collaborators suggested this AS program is rod specific and built an extensive database of AS in human tissue, named ASCOT (Ling et al., 2020). Our AS analysis matches ASCOT findings for the most relevant retinal pathways and disease-associated genes (Figure 6A and Supplementary table 3).

Furthermore, we investigated the MSI1-dependence of the AS events we identified in ROs by using rMAPS2. rMAPS2 takes the rMATS AS results and looks for enrichment in RBP binding motifs among up- and down- regulated isoforms. These analyses revealed that many exons upregulated in ROs are enriched in tandem MSI1-binding motifs in the 50 bp and 125 bp regions downstream to the 5' splice site (Figure 6B). This is in agreement with a defined MSI1-enriched region of 200 bp downstream of the AS exons (14). Interestingly, there were also MSI1 motif peaks at the 3' splice site of downstream exons which could be AS.

To investigate further the discordant behaviour of the AS exons we investigated in the previous section, we compared locations of their MSI1 binding motifs by using RBPmaps (Paz et al., 2014) (Figure 6C). RBPmaps identifies binding motifs for RBPs in sequences of interest. As the novel retinal transcriptome shows conservation across mammals (Ling et al., 2020; Tapial et al., 2017), we hypothesised that regulatory regions would be under the same evolutionary constraints and applied the RBPmaps

bioRxiv preprint doi: https://doi.org/10.1101/2021.08.04.454918; this version posted August 5, 2021. The copyright holder for this preprint (which was not certified by peer review) is the author/funder. All rights reserved. No reuse allowed without permission.

conservation filter, which considers the degree of sequence conservation between human and mouse. *IMPDH1* exon-14, *CC2D2A* exon 30, *ADGRV1* and *CASK* meet the requirements of the majority of MSI1-driven exons, specifically being enriched in MSI1 binding motifs in close proximity to the donor splice site and in PTBP1 binding motifs upstream to the acceptor splice site (Ling et al., 2020; Murphy et al., 2016). Conversely, *CC2D2A* exon 24 has MSI1 tandem motifs further downstream to the 5' splice site while *DOC2B* displays a single motif. Our data suggest these sites might be inactive with respect to regulation of these retinal exons. Surprisingly, *REEP6.1* has putative binding motifs for MSI1; however, they are at the suggested limit of the MSI1 binding range (Figure 6C) (Ling et al., 2020). Moreover, the *REEP6.2* isoform was also reduced, such that this could be independent of retinal specific splicing. This shows a more complex mechanism might regulate splicing in retina, possibly in different cell types, or that another exon which is common to both *REEP6.1* and *REEP6.2* might be affected.

Intriguingly, we noticed the cryptic exon X CEP290-LCA displays long-range downstream MSI1 binding sites similar to those of *REEP6.1* (Figure 6C). Therefore, it is unlikely they could regulate the CEP290-LCA AS splicing pattern. Nonetheless, CEP290-LCA displays a repeated MSI1 motifs cluster upstream of the 3' splice site that is conserved, despite the CEP290-LCA pseudoexon not being a natural exon. This is in accordance with the ASCOT analyses which found that high levels of MSI1 expression can activate non-conserved, otherwise non-expressed, cryptic exons such as in the *RDX* and *GDAP1* genes. Ling et al. found these cryptic exons are unusually enriched in MSI1 sites upstream to the 3' splice site, as well as downstream to the 5' splice site (Ling et al., 2020). The retina has a high level of *MSI1* gene expression and the CEP290-LCA pseudoexon seems to closely fit the MSI1 motifs cluster for cryptic

bioRxiv preprint doi: https://doi.org/10.1101/2021.08.04.454918; this version posted August 5, 2021. The copyright holder for this preprint (which was not certified by peer review) is the author/funder. All rights reserved. No reuse allowed without permission.

exons at the 3' splice site. This prompted us to investigate if MSI1 could affect the retinal mis-splicing in CEP290-LCA.

The role of MSI1 in CEP290 c.2991+1655A>G cryptic exon splicing in LCA10.

The CEP290-LCA10 cryptic exon displays long range MSI1 binding motifs downstream of the cryptic splice site and putative binding motifs for both MSI1 and PTPB1 upstream (Figure 6B). This led us to consider MSI1 as a potential regulator of CEP290-LCA10 aberrant splicing, and the pseudo-exon as a novel target. To test this hypothesis, we differentiated homozygous c.2991+1655A>G CEP290-LCA ROs and treated them with *MSI1*-MO to test if MSI1 plays a role in the aberrant splicing of *CEP290*. We performed a 5-day treatment at D195 of CEP290-LCA RO development, and in control ROs, and quantified the amount of *MSI1* and *IMPDH1* exon-14, as a readout of a successful MSI1 functional knockdown (Figure 7). The *MSI1* transcript was decreased following *MSI1*-MO treatment in CEP290-LCA ROs, and the inclusion of *IMPDH1* exon 14 was reduced similar to control ROs, which confirmed effective reduction of MSI1-dependent splicing (Figure 7A). In contrast, there was only a small non-significant reduction in the inclusion of the CEP290-LCA10 cryptic exon. Furthermore, this was not accompanied by an increase in the WT (exon 26-27) *CEP290* transcript (Figure 7A, B), as was observed when using splice switching therapeutic antisense oligonucleotides for LCA10 (Dulla et al., 2018; Parfitt et al., 2016). Therefore, it appears that MSI1 is not a major driver of the photoreceptor specific switch in CEP290-LCA cryptic exon inclusion and that it is likely other factors have a role.

bioRxiv preprint doi: https://doi.org/10.1101/2021.08.04.454918; this version posted August 5, 2021. The copyright holder for this preprint (which was not certified by peer review) is the author/funder. All rights reserved. No reuse allowed without permission.

DISCUSSION

The impact of alternative splicing on fundamental biological processes, as well as health and disease has become increasingly evident thereby driving the characterization and investigation of the underlying mechanisms. Sequencing techniques have become progressively affordable and have allowed unprecedented insights into AS. The most advanced RNA-seq techniques can capture the dynamic nature of the mammalian transcriptome, which can facilitate gene evolution under pressure. For this reason, the relevance of the plethora of AS identified has been debated, whether it is mostly a mechanism of regulation to determine which gene isoforms are switched off by nonsense mediated decay, or if it actively produces functional alternative transcriptome (Blencowe, 2017; Tress et al., 2017). The development of bioinformatic pipelines and cross-comparisons between published datasets have made it possible to navigate this evolutionary "noise" to extract AS events that are conserved in mammals and of interest to human pathophysiology. Among the AS databases, VastDB (Tapial et al., 2017) and, more recently, ASCOT (Ling et al., 2020), have been key to our understanding of AS in the brain and retina. In particular, the brain shows the most abundant degree of AS and has been under the spotlight since the pioneering studies on microexons and their implication in autism (Irimia et al., 2014). The retina, as part of the CNS, has recently come into focus and an increasing body of evidence points to genetic variants affecting AS associated with inherited blinding conditions; namely, *ABCA4*, *CEP290*, *DYNC2H1* (Khan et al., 2020; Parfitt et al., 2016; Vig et al., 2020).

The c.2991+1655A>G deep intronic change in *CEP290* predominantly affects the retina via an unknown AS mechanism, which exacerbates CEP290 aberrant splicing in photoreceptors (Dulla et al., 2018; Parfitt et al., 2016). Unfortunately, *in vivo*

bioRxiv preprint doi: https://doi.org/10.1101/2021.08.04.454918; this version posted August 5, 2021. The copyright holder for this preprint (which was not certified by peer review) is the author/funder. All rights reserved. No reuse allowed without permission.

humanised animal models of the c.2991+1655A>G LCA10 variant are of limited use, as they do not fully recapitulate *CEP290* aberrant splicing and the human LCA10 phenotype (Garanto et al., 2013). Therefore, we generated hiPSC-derived ROs from a CEP290-LCA patient and healthy control as models of retinal development *in vitro*. We defined the retinal transcriptome by comparing ROs and RPE. Then, we exploited published datasets to cross-compare AS events of interest in ROs and found they are in accordance with the AS Databases. We observed the retinal AS program starts as early as day 20 of ROs development and increases exponentially up to 200 days in culture *in vitro*. We also found MSI1 is an essential driver of AS for many genes in the human retina and defined the constrains for its activity.

Musashi-1 has been shown to be a master regulator of photoreceptor AS both in mouse and in humans (Ling et al., 2020; Murphy et al., 2016; Sundar et al., 2020); therefore, we investigated the dependence of shortlisted exons on MSI1. Knockdown of *MSI1* in ROs shows a direct effect on those exons that strictly met the previously defined MSI1 dependencies (Ling et al., 2020; Murphy et al., 2016). However, *MSI1* knockdown had effects that extended beyond AS alone, through the reduction of *NRL*, *NR2E3* and *CRX*, that has implications for retinal development, photoreceptor function and survival. At present, it is not clear whether the mechanism for this reduction is through a direct effect on these transcripts or by acting via other factors that influence their expression, but it highlights the importance of MSI1 for retinal homeostasis and potential uninvestigated roles. This is in partial agreement with a mouse double conditional knockout for *Msi1* and *Msi2,* which shows defects in photoreceptor morphogenesis, due to impaired outer segment development (Sundar et al., 2020). The conditional pan-retinal *Msi1* and *Msi2* knockouts developed a laminated retina suggesting no major defects in stemness or in photoreceptor specification; however,

bioRxiv preprint doi: https://doi.org/10.1101/2021.08.04.454918; this version posted August 5, 2021. The copyright holder for this preprint (which was not certified by peer review) is the author/funder. All rights reserved. No reuse allowed without permission.

there were alterations in retinal cell survival, including defects in the neuroblastic layer as early as P5. We showed instead that key photoreceptor transcription factors were affected by the *MSI1* knockdown in human retinal organoids, with reduction of *CRX*, *NRL* and *NR2E3* and this could influence retinal development or maintenance. Interestingly, the mouse *Msi1* conditional KO alone had a less pronounced effect on AS or retinal function and survival, perhaps indicating a greater importance for MSI1 in human retina.

Moreover, we found MSI1 seems dispensable for *DOC2B*, *CC2D2A* exon-24 AS and has little effect on the cryptic exon splicing in CEP90-LCA. This suggests that an alternative scenario may exists in human retina and that other RBPs might be involved. For example, PRPF31 has been shown to influence retinal AS in ROs and RPE (Buskin et al., 2018), and several splicing factors have been identified as retinal disease genes. More recently, a study on AS during organ development in mammals highlighted the RBP QKI being at the hinge of AS in heart and brain development (Chen et al., 2021; Mazin et al., 2021). Indeed, the rMAPS2 analysis we performed showed a significant peak for QKI just upstream to the 3' splice sites (Supplementary Figure S1). However, this might be because many AS events we identified share a broader neuronal expression, rather than an exclusively retinal one, such that the link with CEP90-LCA is still missing. Nonetheless, iPSC-derived ROs are a valuable model to faithfully recapitulate conditions affecting AS in human retina, with special relevance to intronic variants and for developing potential therapies (Cideciyan et al., 2019, 2021; Khan et al., 2020; Parfitt et al., 2016).

bioRxiv preprint doi: https://doi.org/10.1101/2021.08.04.454918; this version posted August 5, 2021. The copyright holder for this preprint (which was not certified by peer review) is the author/funder. All rights reserved. No reuse allowed without permission.

EXPERIMENTAL PROCEDURES

Bioinformatic analysis

RNA-Seq analysis of ROs and RPE was carried out as described previously (Lane et al., 2020). Three ROs and RPE replicates from the control BJ line (ATCC CRL-2522) were harvested at D150. The RNA was extracted with the RNeasy micro kit (QIAGEN) following the manufacturer's instructions, followed by paired-end sequencing at 100 million read depth for each sample (Illumina, Otogenetics, Atlanta, GA, USA). Raw.fastq sequences were cleaned from any residual sequencing adapter using cutadapt with parameters -m 20 and -e 0.1. Fragments were then aligned to the human genome (build 38, Ensembl version 92) using STAR. BAM files were then used by rMATS to detect differentially spliced exons in retinal organoids (ROs) compared to the RPE data with settings –novelSS to enable detection of novel splice sites (unannotated splice sites). Sashimi plots were made using the function rmats2sashimiplot.

Online resources and tools.

We exploited different online resources and tools. Namely, VastDB https://vastdb.crg.eu/wiki/Main_Page, ASCOT http://ascot.cs.jhu.edu/, rMAPS2 http://rmaps.cecsresearch.org/ and RBPmap http://rbpmap.technion.ac.il/ and the UCSC Genome Broswer https://genome.ucsc.edu/.

Differentiation of iPSCs to RPE and ROs

RPE was differentiated as in (Schwarz et al., 2015), while ROs were differentiated according to the protocol described by Zhong and collaborators (Zhong et al., 2014); with modifications (de Bruijn et al., 2020; Lane et al., 2020). In brief, iPSCs were grown

bioRxiv preprint doi: https://doi.org/10.1101/2021.08.04.454918; this version posted August 5, 2021. The copyright holder for this preprint (which was not certified by peer review) is the author/funder. All rights reserved. No reuse allowed without permission.

to 95% confluence in E8 medium. Colonies were gently scraped in gentle dissociation buffer (ThermoFisher Scientific) to form embryoid bodies (EBs). EBs were transitioned to neural induction medium in the presence of blebbistatin (Sigma) before seeding at a density of approximately 20 EBs per cm^2. Emerging transparent pouches of neuroepithelium were isolated using a needle or scalpel and cultured in Maturation Medium (3:1 v/v of DMEM: F12, 2% B27 supplement, 1% Non-Essential Amino Acid, 1% Penicillin-Streptomycin, 10% Fetal Bovine Serum (Labtech), 100 µM Taurine, 2 mM GlutaMAX) until day 70, then changed to Retinal Maturation Medium 2 (3:1 v/v of DMEM: F12, 1% N2 supplement, 1% Non-Essential Amino Acid, 1% Penicillin-Streptomycin, 10% Fetal Bovine Serum (Labtech), 100 µM Taurine, 2 mM GlutaMAX). Media was supplemented with 1 µM retinoic acid from day 50 to day 70, then changed to 0.5 µM.

MSI1 knockdown, RNA Extraction and qPCR

The Standard Control and *MSI1* Morpholino (Supplementary Table S4) were designed and synthesized by Gene Tools (Gene Tools, LLC). ROs were mock- or MSI1 treated with 10 µM the *MSI1* Morpholino for 5 days with an additional boost at day 3, following the manufacture protocol.

RNA was extracted from cell lines and retinal organoids using the RNeasy Micro Kit (Qiagen, Hilden, Germany) following the manufacturer's instructions. Then, 50 ng of RNA were converted to cDNA by the Tetro cDNA Synthesis Kit (Bioline, London, UK) and a mixture of oligo-dT and random hexamer primers.

qPCR analysis was performed using the LabTaq Green Hi Rox (Labtech) following manufacturer's instructions on a QuantStudio 6 Flex Real-Time PCR System (Applied Biosystems) and primers listed in Supplementary Table S4.

bioRxiv preprint doi: https://doi.org/10.1101/2021.08.04.454918; this version posted August 5, 2021. The copyright holder for this preprint (which was not certified by peer review) is the author/funder. All rights reserved. No reuse allowed without permission.

Relative gene expression levels were determined with the ΔΔCt method. Statistics and plots were made with GraphPad Prism v.8 (GraphPad Software, Inc.)

Data and Code Availability

The RO and RPE datasets are available at GEO GSE148300 and GSE180531, respectively.

ACKNOWLEDGEMENTS

This work was supported by funding from Retina UK, the Wellcome Trust, Fight for Sight, the NC3Rs and MRC.

AUTHOR CONTRIBUTIONS

D.O., A.L., K.J., J.C.G., P.E.S., K.L.H., A.B.P. and R.G. performed the experiments and/or analysed the data. D.O., A.L., K.J., A.J.H. and M.E.C. conceived the hypothesis and designed the experiments. D.O., A.J.H. and M.E.C. drafted the manuscript. All authors edited the draft manuscript.

DECLARATION OF INTERESTS

The authors declare no competing interests.

bioRxiv preprint doi: https://doi.org/10.1101/2021.08.04.454918; this version posted August 5, 2021. The copyright holder for this preprint (which was not certified by peer review) is the author/funder. All rights reserved. No reuse allowed without permission.

REFERENCES

Arno, G., Agrawal, S.A., Eblimit, A., Bellingham, J., Xu, M., Wang, F., Chakarova, C., Parfitt, D.A., Lane, A., Burgoyne, T., et al. (2016). Mutations in REEP6 Cause Autosomal-Recessive Retinitis Pigmentosa. Am. J. Hum. Genet. *99*, 1305–1315.

Blencowe, B.J. (2017). The Relationship between Alternative Splicing and Proteomic Complexity. Trends Biochem. Sci. *42*, 407–408.

de Bruijn, S.E., Fiorentino, A., Ottaviani, D., Fanucchi, S., Melo, U.S., Corral-Serrano, J.C., Mulders, T., Georgiou, M., Rivolta, C., Pontikos, N., et al. (2020). Structural Variants Create New Topological-Associated Domains and Ectopic Retinal Enhancer-Gene Contact in Dominant Retinitis Pigmentosa. Am. J. Hum. Genet. *107*, 802–814.

Buskin, A., Zhu, L., Chichagova, V., Basu, B., Mozaffari-Jovin, S., Dolan, D., Droop, A., Collin, J., Bronstein, R., Mehrotra, S., et al. (2018). Disrupted alternative splicing for genes implicated in splicing and ciliogenesis causes PRPF31 retinitis pigmentosa. Nat. Commun. *9*, 4234.

Chen, X., Liu, Y., Xu, C., Ba, L., Liu, Z., Li, X., Huang, J., Simpson, E., Gao, H., Cao, D., et al. (2021). QKI is a critical pre-mRNA alternative splicing regulator of cardiac myofibrillogenesis and contractile function. Nat. Commun. *12*, 89.

Cideciyan, A.V., Jacobson, S.G., Drack, A.V., Ho, A.C., Charng, J., Garafalo, A.V., Roman, A.J., Sumaroka, A., Han, I.C., Hochstedler, M.D., et al. (2019). Effect of an intravitreal antisense oligonucleotide on vision in Leber congenital amaurosis due to a photoreceptor cilium defect. Nat. Med. *25*, 225–228.

Cideciyan, A.V., Jacobson, S.G., Ho, A.C., Garafalo, A.V., Roman, A.J., Sumaroka, A., Krishnan, A.K., Swider, M., Schwartz, M.R., and Girach, A. (2021). Durable vision

bioRxiv preprint doi: https://doi.org/10.1101/2021.08.04.454918; this version posted August 5, 2021. The copyright holder for this preprint (which was not certified by peer review) is the author/funder. All rights reserved. No reuse allowed without permission.

improvement after a single treatment with antisense oligonucleotide sepofarsen: a case report. Nat. Med. *27*, 785–789.

Collin, J., Queen, R., Zerti, D., Dorgau, B., Hussain, R., Coxhead, J., Cockell, S., and Lako, M. (2019). Deconstructing Retinal Organoids: Single Cell RNA-Seq Reveals the Cellular Components of Human Pluripotent Stem Cell-Derived Retina. Stem Cells Dayt. Ohio *37*, 593–598.

Craige, B., Tsao, C.-C., Diener, D.R., Hou, Y., Lechtreck, K.-F., Rosenbaum, J.L., and Witman, G.B. (2010). CEP290 tethers flagellar transition zone microtubules to the membrane and regulates flagellar protein content. J. Cell Biol. *190*, 927–940.

den Hollander, A.I., Koenekoop, R.K., Yzer, S., Lopez, I., Arends, M.L., Voesenek, K.E.J., Zonneveld, M.N., Strom, T.M., Meitinger, T., Brunner, H.G., et al. (2006). Mutations in the CEP290 (NPHP6) Gene Are a Frequent Cause of Leber Congenital Amaurosis. Am. J. Hum. Genet. *79*, 556–561.

Dulla, K., Aguila, M., Lane, A., Jovanovic, K., Parfitt, D.A., Schulkens, I., Chan, H.L., Schmidt, I., Beumer, W., Vorthoren, L., et al. (2018). Splice-Modulating Oligonucleotide QR-110 Restores CEP290 mRNA and Function in Human c.2991+1655A>G LCA10 Models. Mol. Ther. Nucleic Acids *12*, 730–740.

Garanto, A., van Beersum, S.E.C., Peters, T.A., Roepman, R., Cremers, F.P.M., and Collin, R.W.J. (2013). Unexpected CEP290 mRNA Splicing in a Humanized Knock-In Mouse Model for Leber Congenital Amaurosis. PLoS ONE *8*.

Irimia, M., Weatheritt, R.J., Ellis, J.D., Parikshak, N.N., Gonatopoulos-Pournatzis, T., Babor, M., Quesnel-Vallières, M., Tapial, J., Raj, B., O'Hanlon, D., et al. (2014). A

bioRxiv preprint doi: https://doi.org/10.1101/2021.08.04.454918; this version posted August 5, 2021. The copyright holder for this preprint (which was not certified by peer review) is the author/funder. All rights reserved. No reuse allowed without permission.

highly conserved program of neuronal microexons is misregulated in autistic brains. Cell *159*, 1511–1523.

Khan, M., Arno, G., Fakin, A., Parfitt, D.A., Dhooge, P.P.A., Albert, S., Bax, N.M., Duijkers, L., Niblock, M., Hau, K.L., et al. (2020). Detailed Phenotyping and Therapeutic Strategies for Intronic ABCA4 Variants in Stargardt Disease. Mol. Ther. Nucleic Acids *21*, 412–427.

Kirschner, R., Rosenberg, T., Schultz-Heienbrok, R., Lenzner, S., Feil, S., Roepman, R., Cremers, F.P., Ropers, H.H., and Berger, W. (1999). RPGR transcription studies in mouse and human tissues reveal a retina-specific isoform that is disrupted in a patient with X-linked retinitis pigmentosa. Hum. Mol. Genet. *8*, 1571–1578.

Kudinov, A.E., Karanicolas, J., Golemis, E.A., and Boumber, Y. (2017). Musashi RNA-Binding Proteins as Cancer Drivers and Novel Therapeutic Targets. Clin. Cancer Res. Off. J. Am. Assoc. Cancer Res. *23*, 2143–2153.

Lancaster, M.A., and Knoblich, J.A. (2014). Organogenesis in a dish: Modeling development and disease using organoid technologies. Science *345*.

Lane, A., Jovanovic, K., Shortall, C., Ottaviani, D., Panes, A.B., Schwarz, N., Guarascio, R., Hayes, M.J., Palfi, A., Chadderton, N., et al. (2020). Modeling and Rescue of RP2 Retinitis Pigmentosa Using iPSC-Derived Retinal Organoids. Stem Cell Rep. *15*, 67–79.

Ling, J.P., Wilks, C., Charles, R., Leavey, P.J., Ghosh, D., Jiang, L., Santiago, C.P., Pang, B., Venkataraman, A., Clark, B.S., et al. (2020). ASCOT identifies key regulators of neuronal subtype-specific splicing. Nat. Commun. *11*, 137.

bioRxiv preprint doi: https://doi.org/10.1101/2021.08.04.454918; this version posted August 5, 2021. The copyright holder for this preprint (which was not certified by peer review) is the author/funder. All rights reserved. No reuse allowed without permission.

Mazin, P.V., Khaitovich, P., Cardoso-Moreira, M., and Kaessmann, H. (2021). Alternative splicing during mammalian organ development. Nat. Genet.

Murphy, D., Singh, R., Kolandaivelu, S., Ramamurthy, V., and Stoilov, P. (2015). Alternative Splicing Shapes the Phenotype of a Mutation in BBS8 To Cause Nonsyndromic Retinitis Pigmentosa. Mol. Cell. Biol. *35*, 1860–1870.

Murphy, D., Cieply, B., Carstens, R., Ramamurthy, V., and Stoilov, P. (2016). The Musashi 1 Controls the Splicing of Photoreceptor-Specific Exons in the Vertebrate Retina. PLoS Genet. *12*, e1006256.

Nakamura, M., Okano, H., Blendy, J.A., and Montell, C. (1994). Musashi, a neural RNA-binding protein required for Drosophila adult external sensory organ development. Neuron *13*, 67–81.

Okano, H., Kawahara, H., Toriya, M., Nakao, K., Shibata, S., and Imai, T. (2005). Function of RNA-binding protein Musashi-1 in stem cells. Exp. Cell Res. *306*, 349–356.

Parfitt, D.A., Lane, A., Ramsden, C.M., Carr, A.-J.F., Munro, P.M., Jovanovic, K., Schwarz, N., Kanuga, N., Muthiah, M.N., Hull, S., et al. (2016). Identification and Correction of Mechanisms Underlying Inherited Blindness in Human iPSC-Derived Optic Cups. Cell Stem Cell *18*, 769–781.

Paz, I., Kosti, I., Ares, M., Cline, M., and Mandel-Gutfreund, Y. (2014). RBPmap: a web server for mapping binding sites of RNA-binding proteins. Nucleic Acids Res. *42*, W361–W367.

bioRxiv preprint doi: https://doi.org/10.1101/2021.08.04.454918; this version posted August 5, 2021. The copyright holder for this preprint (which was not certified by peer review) is the author/funder. All rights reserved. No reuse allowed without permission.

Ruan, G.-X., Barry, E., Yu, D., Lukason, M., Cheng, S.H., and Scaria, A. (2017). CRISPR/Cas9-Mediated Genome Editing as a Therapeutic Approach for Leber Congenital Amaurosis 10. Mol. Ther. J. Am. Soc. Gene Ther. *25*, 331–341.

Schwarz, N., Carr, A.-J., Lane, A., Moeller, F., Chen, L.L., Aguilà, M., Nommiste, B., Muthiah, M.N., Kanuga, N., Wolfrum, U., et al. (2015). Translational read-through of the RP2 Arg120stop mutation in patient iPSC-derived retinal pigment epithelium cells. Hum. Mol. Genet. *24*, 972–986.

Shen, S., Park, J.W., Lu, Z., Lin, L., Henry, M.D., Wu, Y.N., Zhou, Q., and Xing, Y. (2014). rMATS: Robust and flexible detection of differential alternative splicing from replicate RNA-Seq data. Proc. Natl. Acad. Sci. *111*, E5593–E5601.

Sundar, J., Matalkah, F., Jeong, B., Stoilov, P., and Ramamurthy, V. (2020). The Musashi proteins MSI1 and MSI2 are required for photoreceptor morphogenesis and vision in mice. J. Biol. Chem.

Susaki, K., Kaneko, J., Yamano, Y., Nakamura, K., Inami, W., Yoshikawa, T., Ozawa, Y., Shibata, S., Matsuzaki, O., Okano, H., et al. (2009). Musashi-1, an RNA-binding protein, is indispensable for survival of photoreceptors. Exp. Eye Res. *88*, 347–355.

Tapial, J., Ha, K.C.H., Sterne-Weiler, T., Gohr, A., Braunschweig, U., Hermoso-Pulido, A., Quesnel-Vallières, M., Permanyer, J., Sodaei, R., Marquez, Y., et al. (2017). An atlas of alternative splicing profiles and functional associations reveals new regulatory programs and genes that simultaneously express multiple major isoforms. Genome Res. *27*, 1759–1768.

Tress, M.L., Abascal, F., and Valencia, A. (2017). Most Alternative Isoforms Are Not Functionally Important. Trends Biochem. Sci. *42*, 408–410.

bioRxiv preprint doi: https://doi.org/10.1101/2021.08.04.454918; this version posted August 5, 2021. The copyright holder for this preprint (which was not certified by peer review) is the author/funder. All rights reserved. No reuse allowed without permission.

Vig, A., Poulter, J.A., Ottaviani, D., Tavares, E., Toropova, K., Tracewska, A.M., Mollica, A., Kang, J., Kehelwathugoda, O., Paton, T., et al. (2020). DYNC2H1 hypomorphic or retina-predominant variants cause nonsyndromic retinal degeneration. Genet. Med. Off. J. Am. Coll. Med. Genet. *22*, 2041–2051.

Wuebben, E.L., Mallanna, S.K., Cox, J.L., and Rizzino, A. (2012). Musashi2 Is Required for the Self-Renewal and Pluripotency of Embryonic Stem Cells. PLoS ONE *7*.

Zhong, X., Gutierrez, C., Xue, T., Hampton, C., Vergara, M.N., Cao, L.-H., Peters, A., Park, T.-S., Zambidis, E.T., Meyer, J.S., et al. (2014). Generation of three dimensional retinal tissue with functional photoreceptors from human iPSCs. Nat. Commun. *5*, 4047.

bioRxiv preprint doi: https://doi.org/10.1101/2021.08.04.454918; this version posted August 5, 2021. The copyright holder for this preprint (which was not certified by peer review) is the author/funder. All rights reserved. No reuse allowed without permission.

FIGURE TITLES AND LEGENDS

Figure 1. Alternatively spliced genes in 3D retinal organoids (ROs) compared to the RPE (A) Top 20 upregulated AS genes in ROs compared to the RPE. The *IMPDH1* exon 14 is highlighted in bold and was selected as a reporter for AS events. Right panel illustrates exon inclusion in ROs compared to RPE (*CC2D2A*, *IMPDH1*, *REEP6.1* and *TTC8*) **(B)** Top 20 downregulated AS genes in ROs compared to the RPE**.** Right panel illustrates exons more common in RPE compared to ROs (*RALGAPA1*, *BAZ2B*, *PPHLN1* and *ZEB1*).

Figure 2. Temporal resolution of retina-specific exons in retinal organoids. (A) RT-PCR of control RO retinal differentiation markers *PAX6*, *VSX2*, *CRX*, *NRL* and *NR2E3*. **(B)** qPCR semi-log plots showing their temporal expression in control retinal organoids at day 20, 40, 70, 90, 100, 150, 180, 200 (mean of n≥3 experiments ± SD for each time point).

Figure 3. Temporal resolution of retina-specific exons in retinal organoids. (A) RT-PCR of control RO retinal-specific exons in *BBS8* (*BBS8* exon-2A), *REEP6.1* (upper band), *REEP6.2* (lower band), *RPGRorf15* and *IMPDH1* exon-14. **(B)** qPCR semi-log plots showing their temporal expression in control ROs at day 20, 40, 70, 90, 100, 150, 180, 200 (mean of n≥3 experiments ± SD for each time point).

Figure 4. qPCR analysis for markers of retinal differentiation in control organoids treated with the MSI1-Morpholino

bioRxiv preprint doi: https://doi.org/10.1101/2021.08.04.454918; this version posted August 5, 2021. The copyright holder for this preprint (which was not certified by peer review) is the author/funder. All rights reserved. No reuse allowed without permission.

qPCR analysis of markers of retinal differentiation *VSX2, PAX6*, *NRL, NR2E3* and *CRX* (Panel A-F) in control ROs treated with 10 μM of the MSI1-Morpholino (*MSI1*-MO) for 5 days. The MSI1 knockdown effect is highlighted with solid square as reference for working *MSI1*-MO. For each gene, the graph on the right shows fold-changes compared to the mean of control-MO treated (CTL) ROs; individual replicates are plotted as reciprocal of the dCt values used to calculate the fold-changes. Statistics was performed on dCt values by Student t-test with the GraphPad Prism 5 software. (mean of n=9 organoids ± SD. Each point represents an individual organoid. *P≤0.05, **P≤0.01,***P≤0.001, unpaired, two-tailed, Student's t-test).

Figure 5. qPCR analysis for retinal-specific exons of control organoids treated with the MSI1-Morpholino

qPCR analysis of retinal-specific exons in *IMPDH1* exon-14, *CC2D2A* exon 24 and 30, *CASK*, *ADGRV1*, *DOC2B, REEP6.1* and *REEP6.2* (Panel A-F) in control ROs treated with the MSI1-Morpholino treated with 10μM of MSI1-MO for 5 days (*MSI1*-MO). For each gene, the graph on the right shows fold-changes compared to the mean of control-MO treated (CTL) ROs; individual replicates are plotted as reciprocate of the dCt values used to calculate the fold-changes. Statistics was performed on dCt values by Student t-test with the GraphPad Prism 5 software. (mean of n=9 organoids ± SD. Each point represents an individual organoid. *P≤0.05, **P≤0.01,***P≤0.001, unpaired, two-tailed, Student's t-test).

Figure 6. Analysis of selected retinal-specific exons and CEP290-LCA cryptic exon. (A) AS events in selected genes in ROs that match those identified by Ling and colleagues in ASCOT (Ling et al., 2020). **(B)** rMAPS2 analysis of the enrichment in

bioRxiv preprint doi: https://doi.org/10.1101/2021.08.04.454918; this version posted August 5, 2021. The copyright holder for this preprint (which was not certified by peer review) is the author/funder. All rights reserved. No reuse allowed without permission.

MSI1 binding motifs in upregulated (Enhanced, red line) and downregulated, skipped (Silenced, blue line) and up/downstream of the 3' and 5' splice sites, respectively. **(C)** RBPmaps analysis displayed on the UCSC Genome Browser shows the locations of MSI1 binding motifs (red peaks) and PTPB1 binding motifs (blue peaks). The peak heights reflect different significance of the RBPmaps results (the higher the peak, the smaller the p-value, p-value cutoff < 0.01). The RefSeq is shown along with the retina RNA-Seq used to build ASCOT (Ling et al., 2020), as some of the exons are not yet annotated. IMPDH1 exon-14, CC2D2A exon 24 and 30**,** DOC2B, ADGRV1, CASK, REEP6.1 and CEP290-LCA cryptic exon are reported.

Figure 7. qPCR analysis of CEP290-LCA retinal organoids treated with the MSI1-Morpholino.

(A) qPCR analysis of *MSI1*, *IMPDH1* exon 14, CEP290 cryptic and canonical isoforms in D195 CEP290-LCA retinal organoids treated with 10µM of MSI1-MO for 5 days. The MSI1 knockdown effect is highlighted with a red square and used as a reference for successful knockdown with the *MSI1*-MO. For each gene, the graph on the right shows fold-changes compared to the mean of control-MO treated (CTL) ROs; individual replicates are plotted as reciprocate of the dCt values used to calculate the fold-changes. Statistics was performed on dCt values by Student t-test with the GraphPad Prism 5 software. (mean of n=3 organoids ± SD. Each point represents an individual organoid. *P≤0.05, **P≤0.01,***P≤0.001, unpaired, two-tailed, Student's t-test). **(B)** RT-PCR image analysis of *MSI1*, *IMPDH1* exon 14, CEP290 cryptic and canonical isoforms in CEP290-LCA retinal organoids treated with MSI1-MO.

bioRxiv preprint doi: https://doi.org/10.1101/2021.08.04.454918; this version posted August 5, 2021. The copyright holder for this preprint (which was not certified by peer review) is the author/funder. All rights reserved. No reuse allowed without permission.

SUPPLEMENTAL INFORMATION

Supplementary Table S1. rMATS Alternative splicing results. Exons with significant difference in the inclusion levels in retinal organoids (ROs) compared to the RPE are highlighted**.**

Supplementary Table S2. rMATS Alternative splicing results and filtered for orthologues. Exons with significant difference in the inclusion levels in retinal organoids (ROs) compared to the RPE shortlisted for events identified in mice (Murphy et al., 2015)**.**

Supplementary Table S3. Alternative splicing analysis. Exons with significant difference in the inclusion levels in retinal organoids (ROs) compared to the RPE and matched to those shortlisted in ASCOT (Ling et al., 2020)**.**

Supplementary Table S4. Morpholino and Primer sequences for RT and qPCR.

Supplementary Figure S1. rMAPS2 analysis of the enrichment in QKI binding motifs in upregulated (Enhanced, red line) and downregulated, skipped (Silenced, blue line) and up/downstream of the 3’ and 5’ splice sites, respectively

bioRxiv preprint doi: https://doi.org/10.1101/2021.08.04.454918; this version posted August 5, 2021. The copyright holder for this preprint (which was not certified by peer review) is the author/funder. All rights reserved. No reuse allowed without permission.

A

Top 20 *upregulated* retinal exons

#	Symbol	AS exon coordinates (hg38)	Inclusion Level Difference
1	AGAP1	chr2:235718380-235718392:+	0.901
2	CAMSAP1	chr9:135865331-135865364:-	0.876
3	CAMSAP1	chr9:135863775-135863847:-	0.865
4	DDHD1	chr14:53096116-53096218:-	0.859
5	CC2D2A	chr4:15576603-15576624:+	0.843
6	MBNL2	chr13:97365135-97365171:+	0.8
7	**IMPDH1**	**chr7:128393721-128393738:-**	**0.754**
8	REEP6	chr19:1496590-1496671:+	0.704
9	TTC8	chr14:88833692-88833722:+	0.679
10	RIMS2	chr8:104094477-104094729:+	0.664
11	MBNL2	chr13:97365135-97365171:+	0.652
12	SSR1	chr6:7295087-7295102:-	0.635
13	ADD1	chr4:2926641-2926675:+	0.617
14	EFR3A	chr8:131988689-131988740:+	0.605
15	ERGIC3	chr20:35554371-35554386:+	0.598
16	SGIP1	chr1:66694438-66694504:+	0.597
17	TPD52	chr8:80050444-80050471:-	0.58
18	CLIP1	chr12:122276438-122276444:-	0.558
19	CAMSAP1	chr9:135863787-135863847:-	0.519
20	FRYL	chr4:48598828-48598873:-	0.515

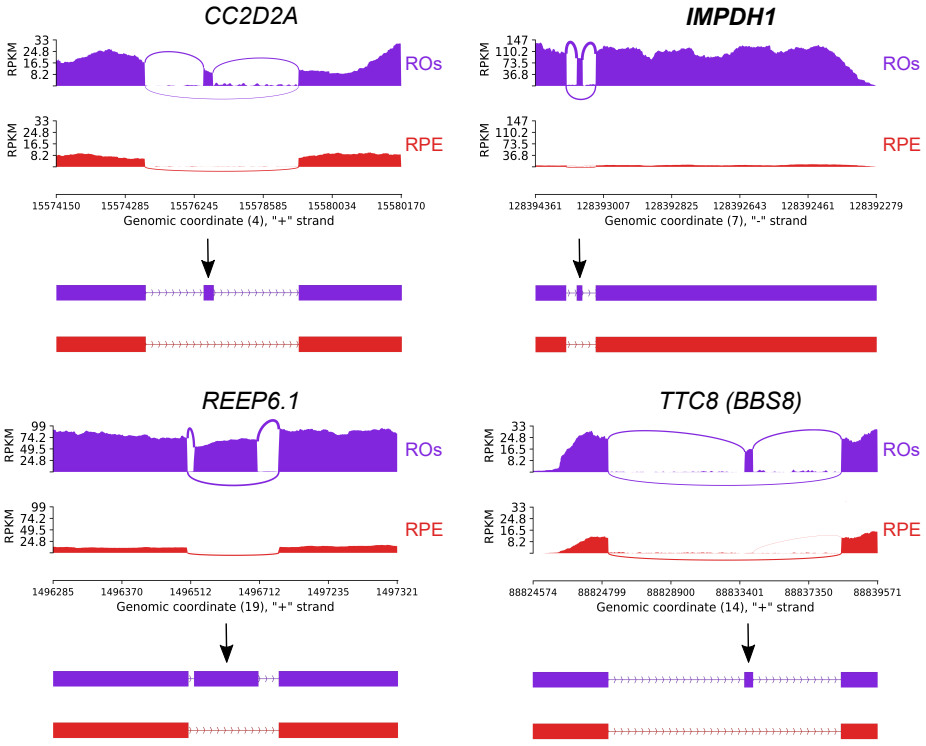

B

Top 20 *downregulated* retinal exons

#	Symbol	AS exon coordinates (hg38)	Inclusion Level Difference
1	CCDC136	chr7:128810138-128810366:+	-0.894
2	PROM1	chr4:15979394-15979463:-	-0.889
3	RALGAPA1	chr14:35548507-35548538:-	-0.759
4	BAZ2B	chr2:159397073-159397100:-	-0.704
5	CACNB2	chr10:18514235-18514369:+	-0.703
6	PPHLN1	chr12:42384939-42384996:+	-0.646
7	BAZ2B	chr2:159397067-159397100:-	-0.645
8	IQSEC1	chr3:13047477-13047522:-	-0.566
9	DPF3	chr14:72669951-72671338:-	-0.52
10	ZEB1	chr10:31373017-31373173:+	-0.503
11	KIF21A	chr12:39330241-39330262:-	-0.502
12	CAMSAP1	chr9:135863787-135863847:-	-0.499
13	ZEB1	chr10:31387123-31387266:+	-0.468
14	WASF3	chr13:26680034-26680201:+	-0.468
15	WASF3	chr13:26680034-26680201:+	-0.407
16	GPHN	chr14:66985681-66985738:+	-0.402
17	TPD52L2	chr20:63875815-63875875:+	-0.346
18	MEIS2	chr15:36894716-36894812:-	-0.319
19	PROM1	chr4:15979880-15979904:-	-0.318
20	CLIP1	chr12:122336631-122336748:-	-0.31

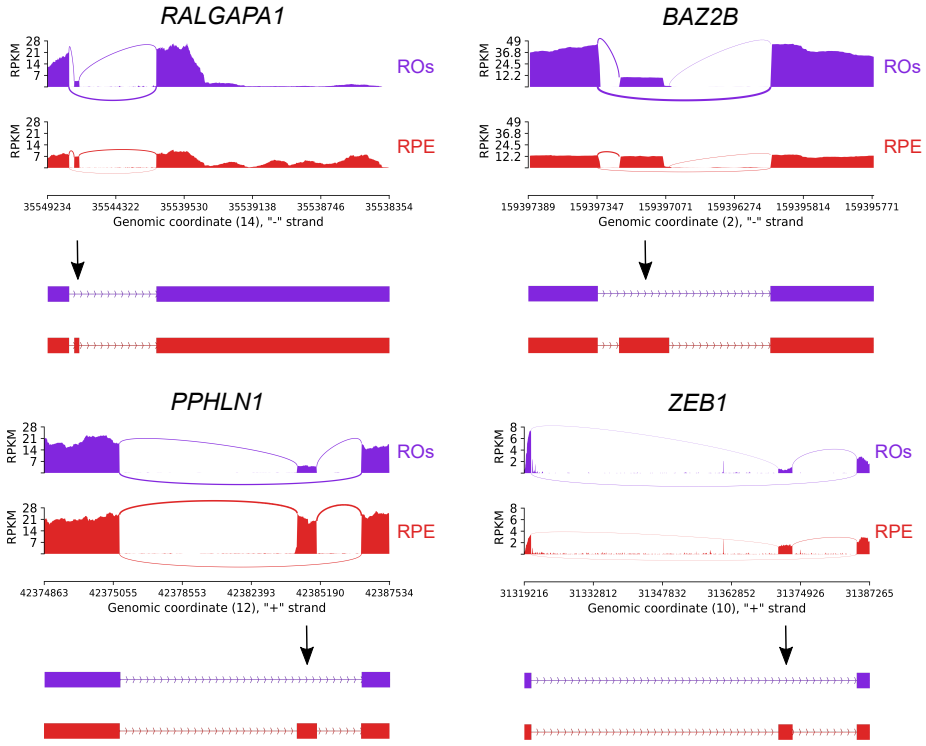

bioRxiv preprint doi: https://doi.org/10.1101/2021.08.04.454918; this version posted August 5, 2021. The copyright holder for this preprint (which was not certified by peer review) is the author/funder. All rights reserved. No reuse allowed without permission.

A

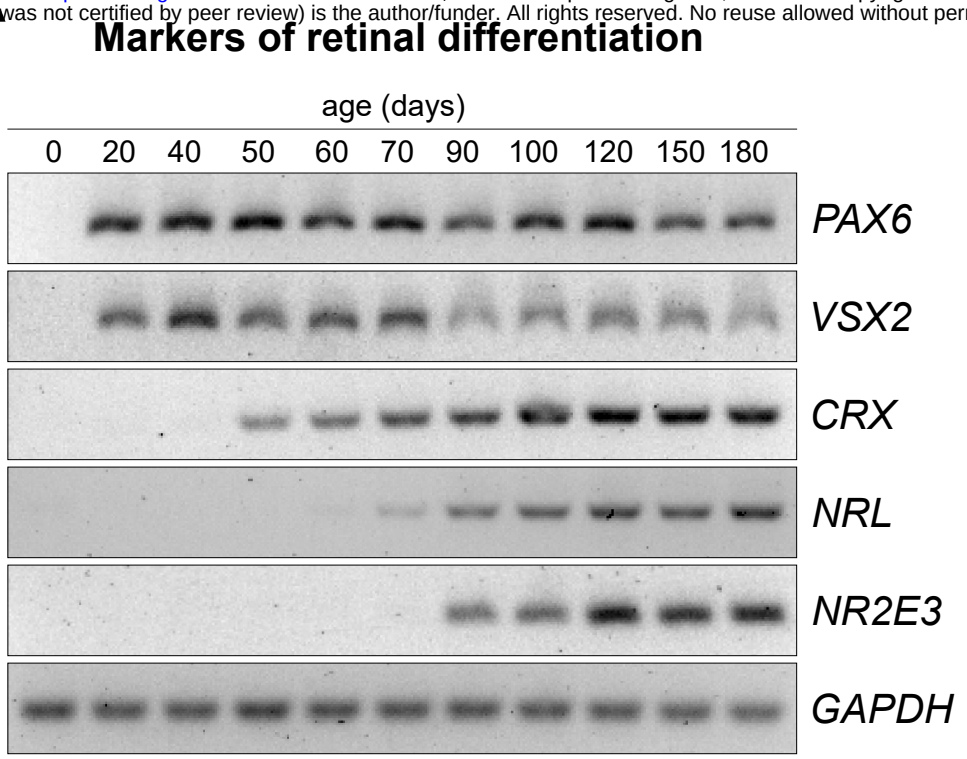

B

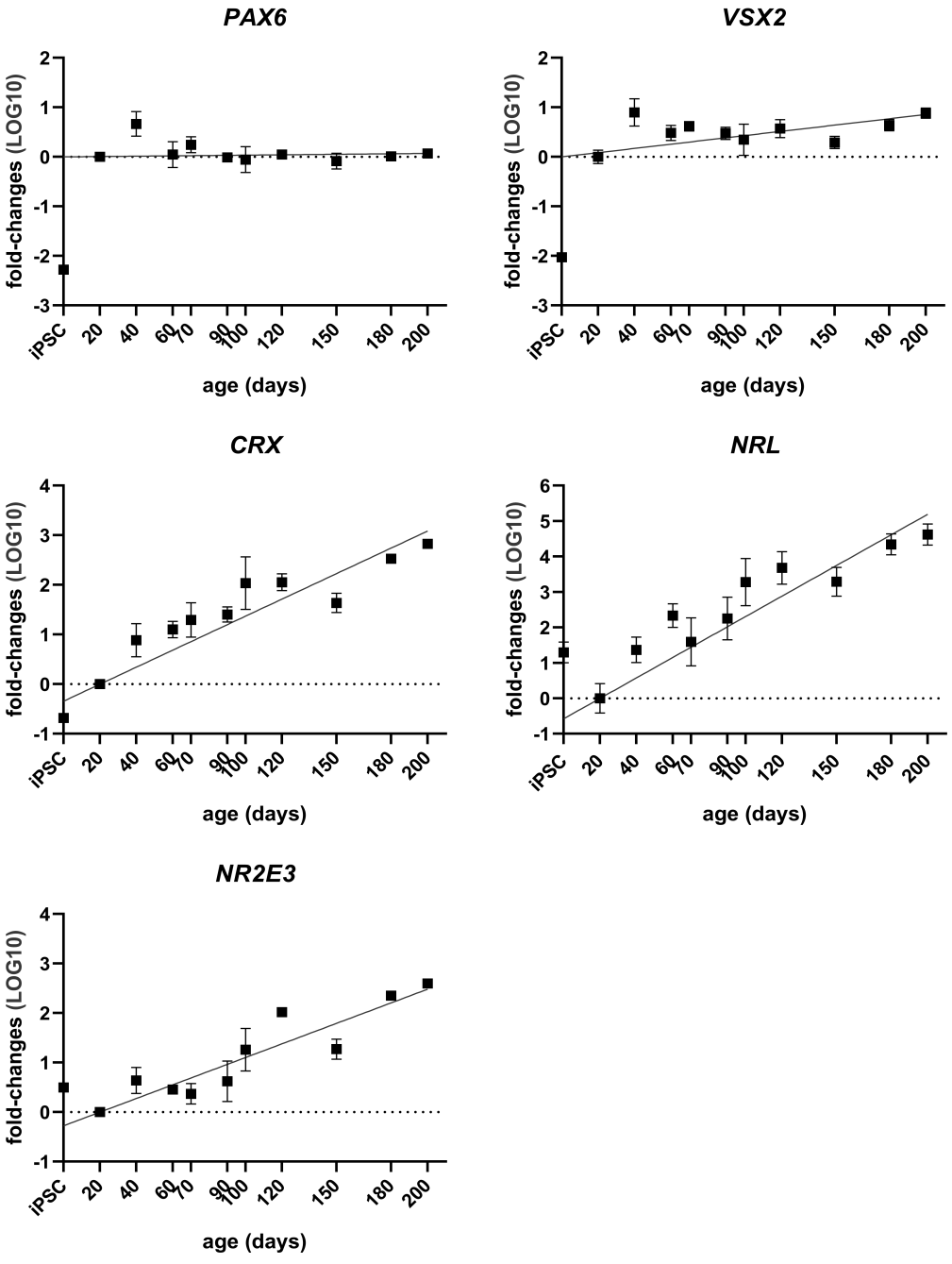

bioRxiv preprint doi: https://doi.org/10.1101/2021.08.04.454918; this version posted August 5, 2021. The copyright holder for this preprint (which was not certified by peer review) is the author/funder. All rights reserved. No reuse allowed without permission.

A

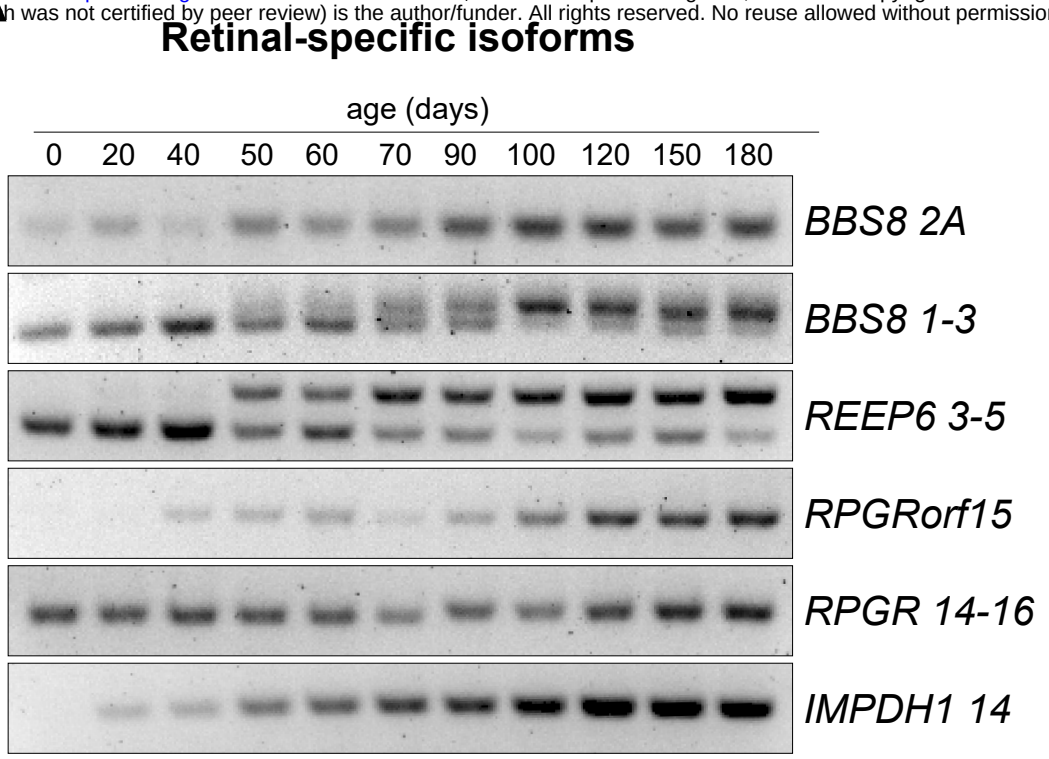

B

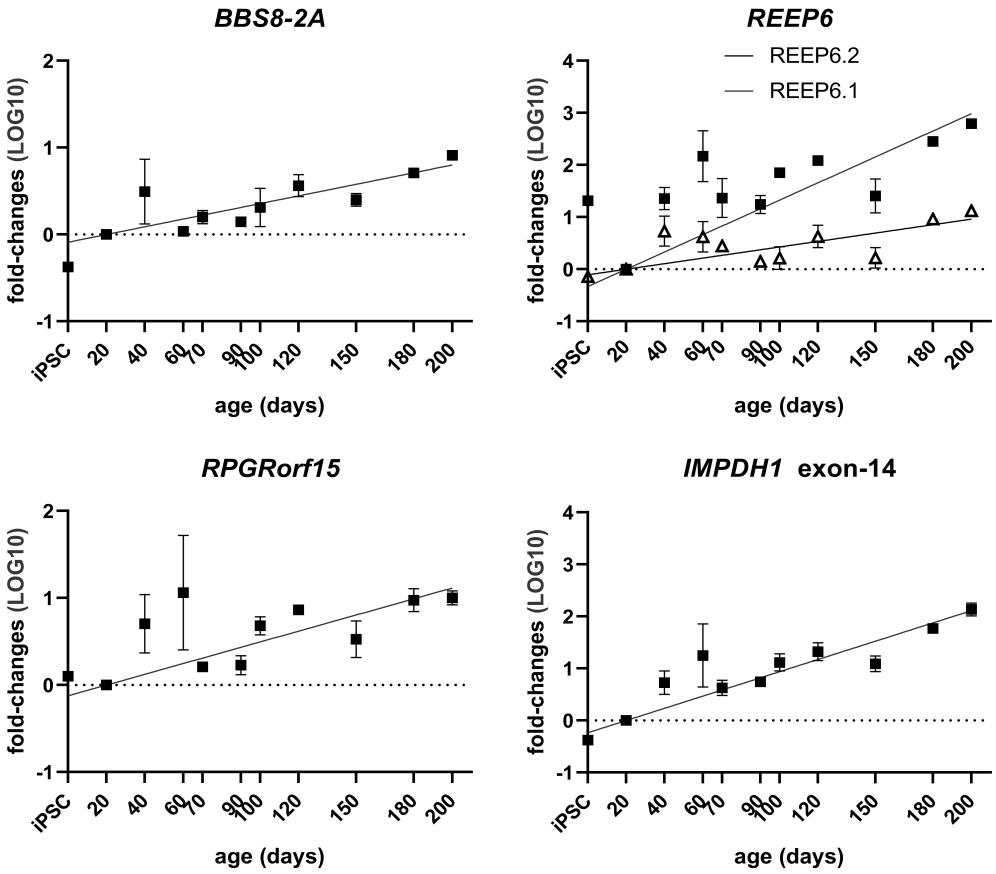

bioRxiv preprint doi: https://doi.org/10.1101/2021.08.04.454918; this version posted August 5, 2021. The copyright holder for this preprint (which was not certified by peer review) is the author/funder. All rights reserved. No reuse allowed without permission.

Markers of retinal differentiation

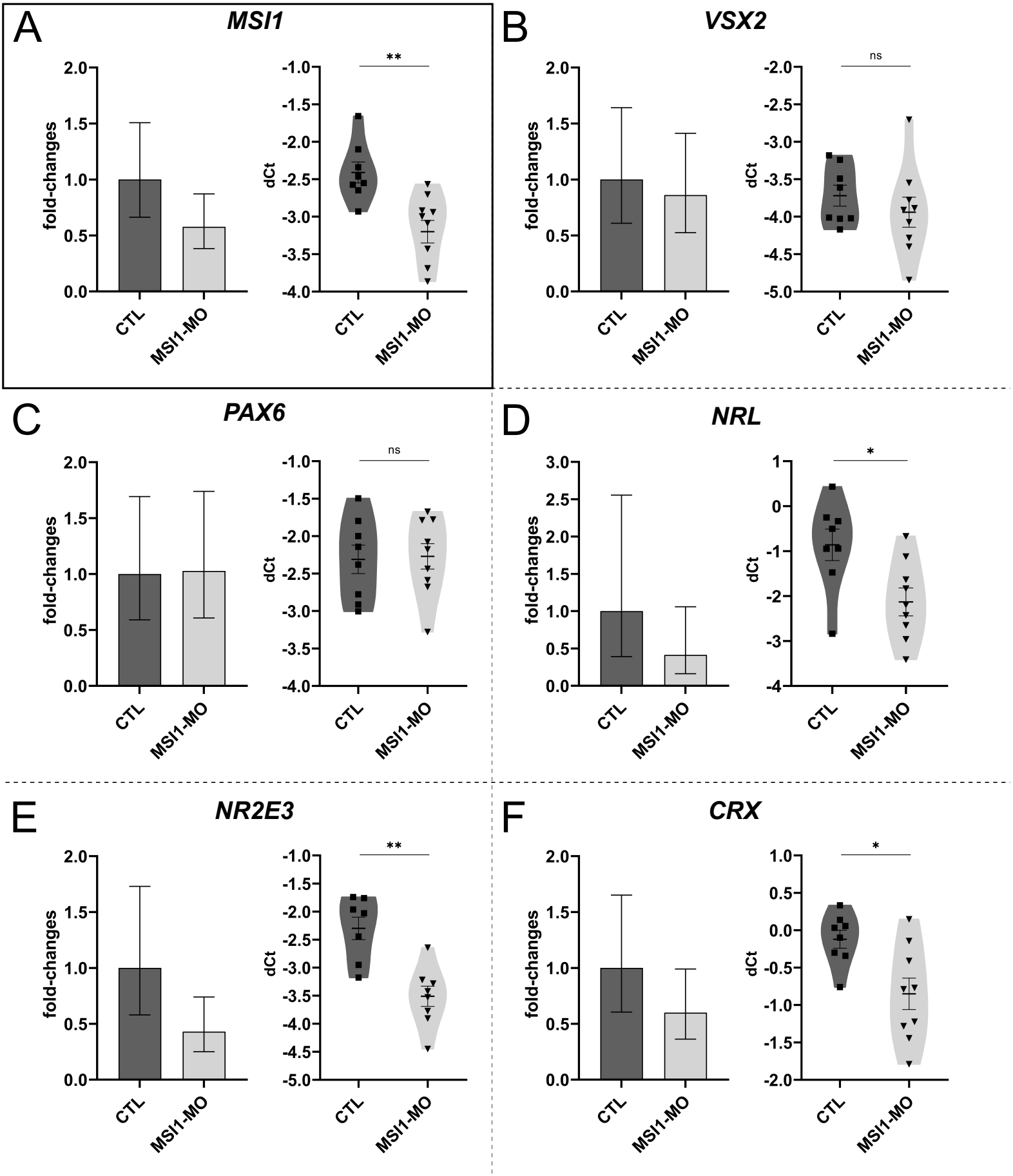

bioRxiv preprint doi: https://doi.org/10.1101/2021.08.04.454918; this version posted August 5, 2021. The copyright holder for this preprint (which was not certified by peer review) is the author/funder, all rights reserved. No reuse allowed without permission.

MSI1-dependent isoforms

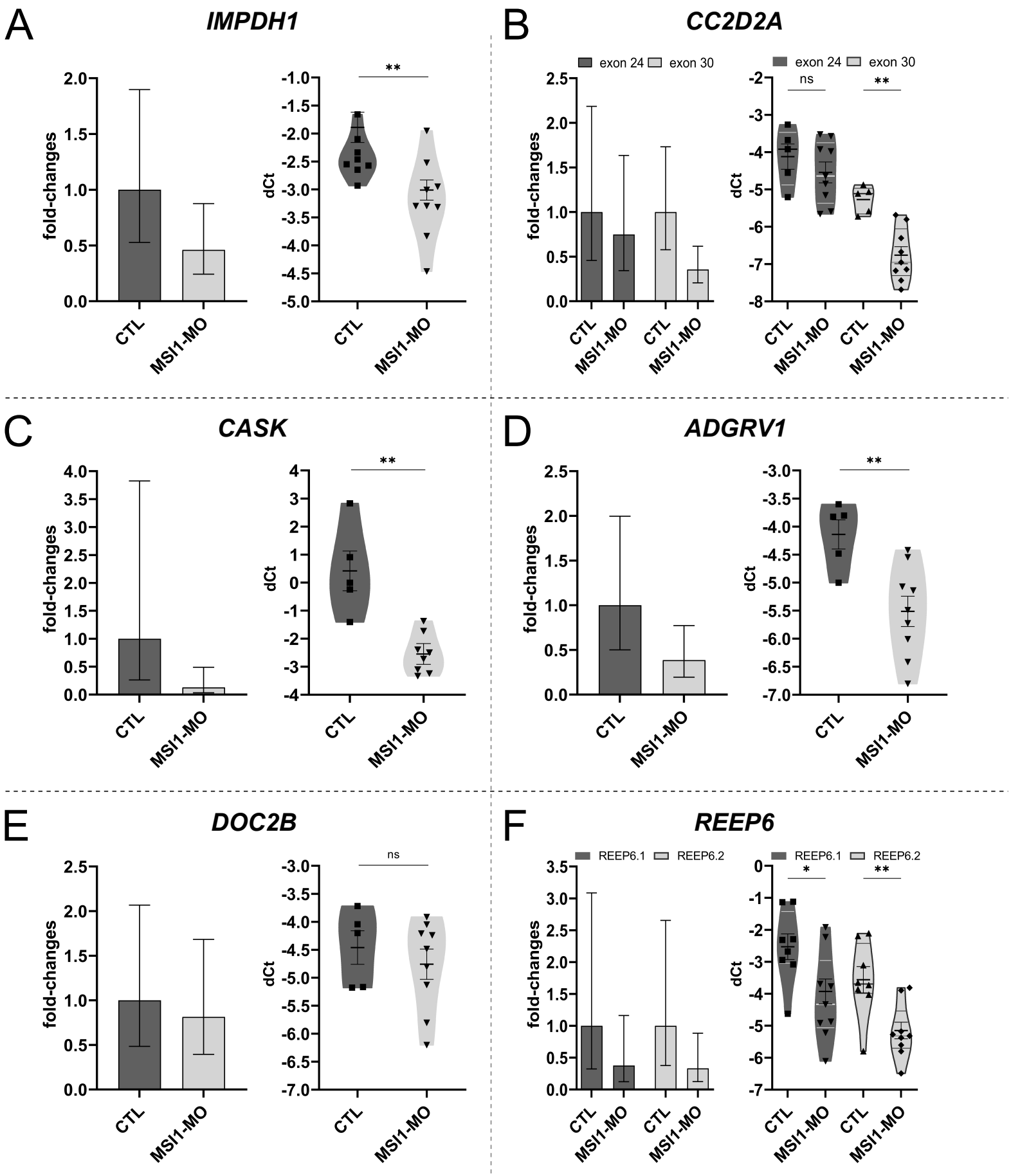

bioRxiv preprint doi: https://doi.org/10.1101/2021.08.04.454918; this version posted August 5, 2021. The copyright holder for this preprint (which was not certified by peer review) is the author/funder. All rights reserved. No reuse allowed without permission.

A

Gene	Genes with rod-specific exons	Associated diseases	Murphy *et al. (7)*
IFT140	Cilia Formation	Retinitis Pigmentosa	NO
CC2D2A			YES
CC2D2A			NO
TTC8			YES
ADGRV1			NO
CASK	Neuronal Synapse	Intellectual disability	NO
KIF1B			NO
DOC2B			NO
STXBP5			NO
BSG	Metabolism		YES
SLC4A7			NO
GRAMD1B	JAK/STAT & AKT pathways		NO
KCTD5			NO

Gene	Genes with rod-specific exons	Associated diseases	Murphy *et al. (7)*
IMPDH1	G protein signaling pathway	Retinitis Pigmentosa	YES
EFR3A			YES
FARP2			NO
KMT2D	Transcription & splicing		YES
INTS13			NO
MSI2			NO
PPP3CC	Other		NO
PLEKHB1			NO
MAN2A2			NO
MARCH1			NO
HCN1			NO
DMD		Duchenne muscular dystrophy	NO

B

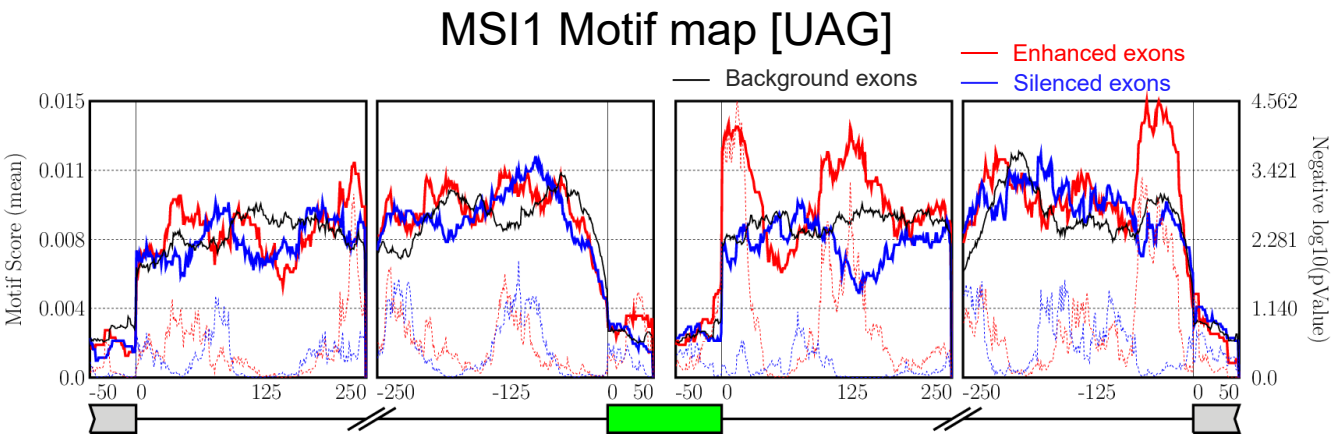

C

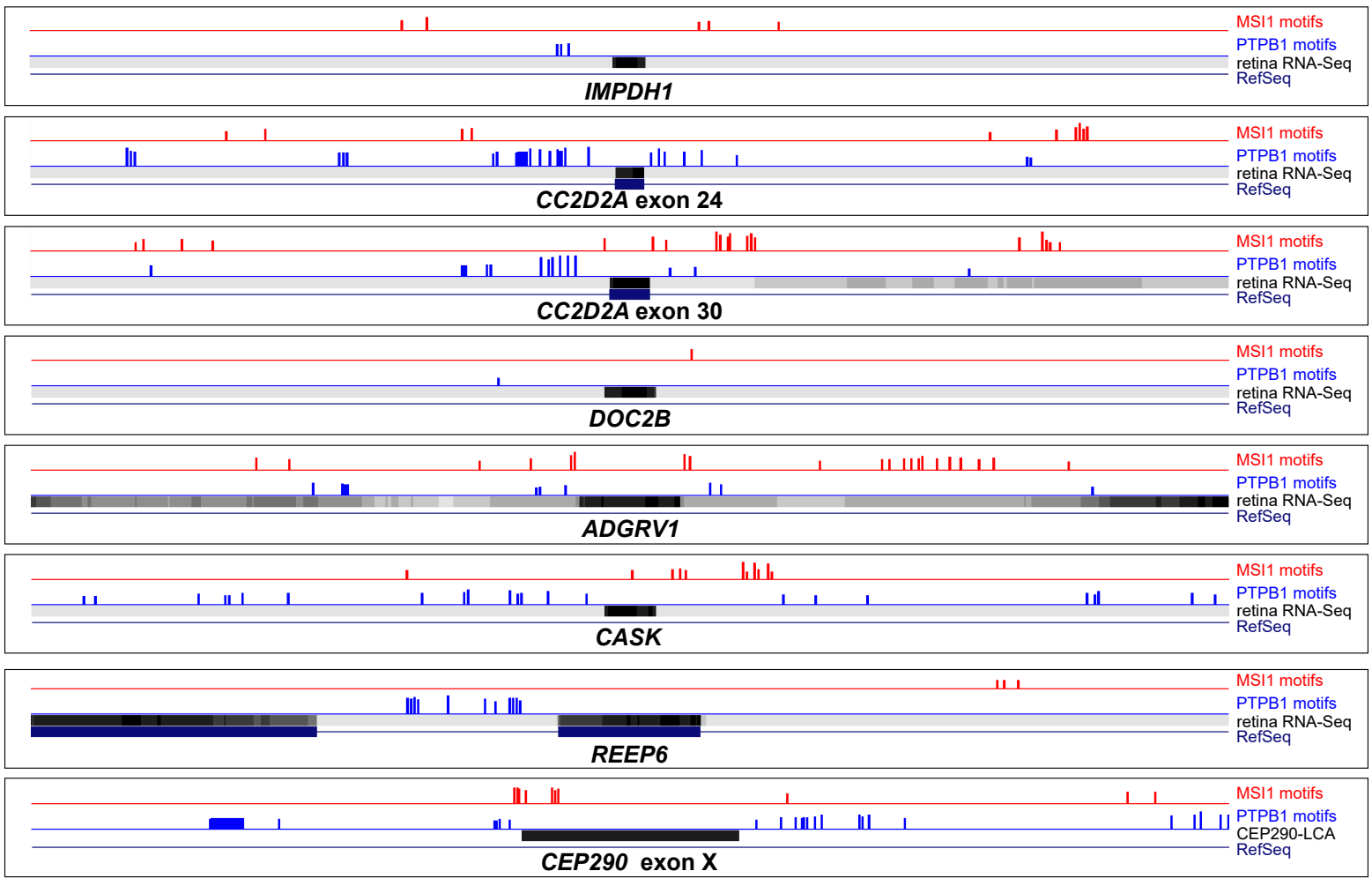

bioRxiv preprint doi: https://doi.org/10.1101/2021.08.04.454918; this version posted August 5, 2021. The copyright holder for this preprint (which was not certified by peer review) is the author/funder. All rights reserved. No reuse allowed without permission.

A

MSI1 Knockdown in CEP290-LCA Retinal Organoids

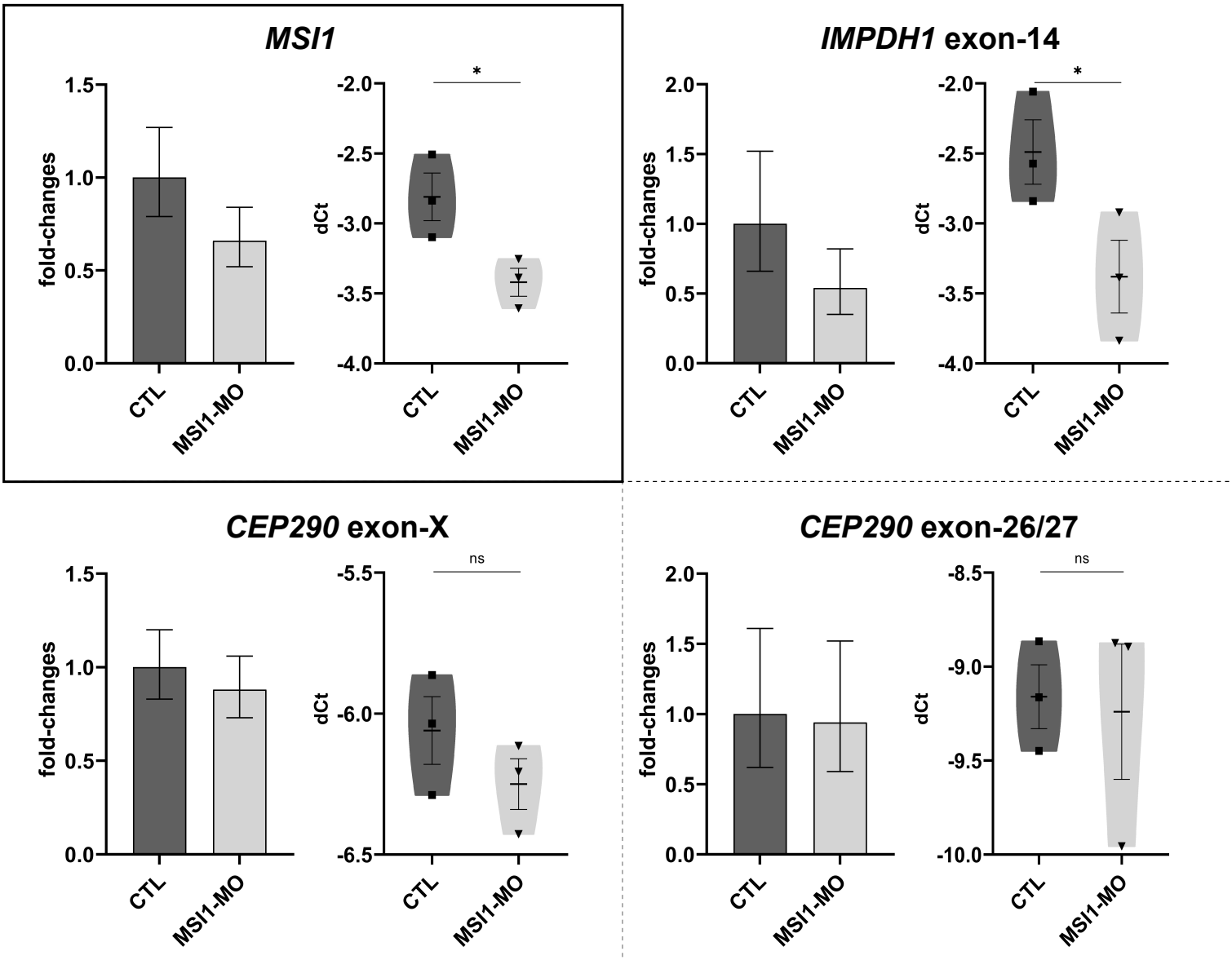

B